Single-stage Grid-Connected PV System with Finite Control Set Model Predictive Control and an Improved Maximum Power Point Tracking

Simone Vanti, *Student Member IEEE,* Prabhat Ranjan Bana, *Student Member IEEE,* Salvatore D'Arco and Mohammad Amin, *Senior Member IEEE*

***Abstract*—The single-stage grid-connected photovoltaic (PV) topology has recently drawn attention as it can reduce overall losses and installation costs. This paper presents a new control approach for single-stage grid-connected PV systems. The proposed controller is a combination of a finite control set model predictive control (FCS-MPC) and a maximum power point tracking (MPPT) algorithm, which ensures the extraction of maximum power from the PV panels and good transient performance for the output voltage and current. The disadvantages of classical MPPT algorithms in tracking the global maximum power point under fluctuating environmental conditions are avoided by including additional constraints in the cost function of the FCS-MPC. Further, the controller is tested for partial shading in PV. The performance of the proposed controller is compared with the two-stage and single-stage PV configuration with different controls and MPPT algorithms. The simulation results show that the single-stage PV system with the proposed control can effectively extract the maximum power from the PV system and maintain a stable output signal for the transient condition. Finally, experimental results according to a control hardware-in-the-loop (C-HIL) approach are presented to validate the effectiveness of the proposed algorithm.**

***Index Terms*—Model predictive control (MPC), Maximum power point tracking (MPPT), Solar photovoltaic (PV) generation, Voltage source converter (VSC).**

I. Introduction

OVER the last decade, the utilization of the solar energy sector is growing at a much faster pace than the rest of the economy worldwide [1]. Grid-tied inverters are the key solution to connect the PV panels to the utility grid. Two typical configurations of the grid-tied PV system are the single-stage and the two-stage configurations [2].

The two-stage configuration is presented in Fig.1. The system consists of a solar panel, a dc-dc boost converter and an inverter. A three-level neutral point clamped (3L NPC) inverter is shown in Fig. 1, however, it can be any other inverter from two-level to multi-level. The boost converter placed before the three-phase inverter implements a maximum power point tracking (MPPT) to extract the maximum power from the solar panel. The MPPT algorithm generates the duty cycle for the switch of the boost converter that drives the panel dc voltage, v_{pv}. Therefore, the inverter dc voltage, v_{dc} is independent of the panel dc voltage v_{pv}. With a fixed value of v_{dc}, the control system of the inverter is easy to implement, however, the efficiency and the robustness of the entire system is reduced and the installation cost is increased due to the two-stage conversion.

The single-stage configuration shown in Fig. 2 uses only one power converter, which leads to higher efficiency and lower costs compared with the two-stage topology. Nevertheless, the control strategy should be designed to extract the maximum possible power and accurately transfer it from the PV array to the grid with low losses. Several different implementations of single-stage grid-connected PV systems can be found in the literature. A general review of single-phase single-stage PV topologies is presented in [3], focusing on the configuration of the boost converter. Applications for the three-phase systems, with pulse width-modulator (PWM) control and using a fuzzy logic controller are presented in [4] and [5], respectively.

The conventional way of realizing the overall PV voltage source converter (VSC) control structure is by cascaded linear regulators and a PWM [6], [7], as shown in Fig. 1. However, this approach has some limitations such as limited control bandwidth due to the cascaded configuration, slow response as well as risk of stability and interaction issues [8]. To overcome the limitations of the classical control, significant research has been dedicated to Model Predictive Control (MPC) for its fast dynamic response and capability to incorporate constraints in the control law. The main idea behind the MPC is the use of a discrete-time model of the system to forecast the future behavior of the controlled parameter during a certain time window called a receding horizon [9], [10]. The future error between predicted output and the reference value is minimized by using a predefined cost function and the optimal actuation is chosen for the next sample time.

Finite Control Set (FCS) and Continuous Control Set (CCS) MPCs are the two most used MPC implementations [11]. In general, the FCS-MPC is preferred because of its simplicity. It also eliminates using a PWM modulator; however, this control scheme can produce a comparatively higher THD level. One possible approach to avoid this latter issue is the deployment

Manuscript received April xx, 2021 and revised August xx, 2021; accepted November xx, 2021. (Corresponding author: Mohammad Amin.)

Simone Vanti is with the Department of Management and Engineering at the University of Padua, Padova, 35122, Italy, e-mail: simone.vanti@studenti.unipd.it

Prabhat Ranjan Bana is with the Department of Electric Power Engineering at the Norwegian University of Science and Technology, Trondheim, 7491, Norway, e-mail: prabhat.r.bana@ntnu.no

Salvatore D'Arco is with the SINTEF Energy Research, Trondheim, 7465, Norway, e-mail: salvatore.darco@sintef.no

Mohammad Amin is with the Department of Electric Power Engineering at the Norwegian University of Science and Technology, Trondheim, 7491, Norway, e-mail: mohammad.amin@ntnu.no

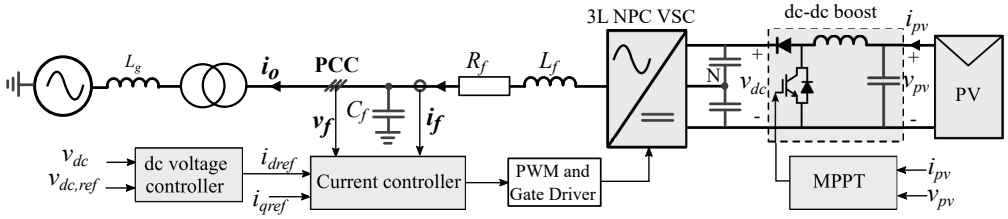

Fig. 1. Schematic of the widely-used two-stage grid-tied PV system.

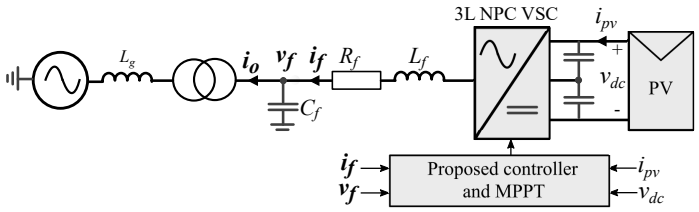

Fig. 2. Schematic of the single-stage grid-tied PV system with the proposed control system.

of longer prediction horizons with the drawback of more computational time needed [12], [13]. However, advanced switching state selection algorithms like sphere coding can be implemented [14], [15]. Moreover, for better performance, the time delay needed by the digital processor to compute the control-law based on the FCS-MPC algorithm could be evaluated. Solutions as shifting one period forward the discrete time model [16] [17] could be applied for the compensation of the computational time. The MPC control has been demonstrated in literature for a wide range of applications as the control of induction machine [18], flux and power control [19], and speed regulation [20], however, the MPC has not been applied to a single-stage PV system.

The main contribution of this paper is presenting a single-stage grid-connected PV system with an FCS-MPC and an improved MPPT technique. The single-stage PV system with the proposed control can track the maximum power point (MPP) even under partially shaded conditions. Possible shaded conditions usually generate multiple peaks in the power-voltage $(p-v)$ curve in a PV array. The classic MPPT algorithms [21], [22] are unable to track the MPP, therefore, an improved MPPT algorithm has been developed to extract the maximum power for this single-stage application. For the evaluation of the results, a numerical comparison between the two-stage configuration with the classical vector PI current control and the proposed single-stage solution is presented for a $100kW$ PV array connected to a $25kV$ grid via a three-phase 3L NPC VSC. Furthermore, the performance of the proposed control is compared for the single-stage configuration in terms of effective MPPT tracking with two other controllers which are (i) a PI current controller combined with the perturb and observe (P&O) MPPT technique and (ii) the CCS-MPC combined with the P&O MPPT technique, considering the works of literature [22]–[24]. The simulations are carried out with linear irradiance changes and with partially shaded conditions to show the capability of the system to work within the entire $p-v$ curve. The performance of the proposed approach is also tested with real irradiance and temperature data coming from a recording of an example of a winter day. The aforesaid prominent vital features of the proposed algorithm are also tested experimentally according to the control hardware-in-loop (C-HIL) approach considering different dynamic test cases to validate the robust operation.

The rest of the paper is organized in the following. Section II presents the analytical modeling and control of the system. Section III presents the modeling of the improved MPPT technique. The simulation results have been discussed in Section IV and the C-HIL test is presented in Section V. Finally, the paper is concluded in Section VI.

II. Analytical Modeling of the VSC and its Control System

In this section, the modeling and control implementation for a single-stage solar PV system are presented.

A. Overview of the FCS-MPC

The FCS-MPC is the most significant predictive control technique for power electronic converters. The approach is based on an optimization problem in which the power converters finite number of switching states is used. In principle, the Predictive Control uses a discrete-time model of the system to forecast the future behavior of the control variables during a certain time window called a receding horizon [9]. The system prediction model can be expressed in state-space form as:

$$x(k+1) = Ax(k) + Bu(k) \tag{1}$$

$$y(k) = Cx(k) + Du(k) \tag{2}$$

where $x(k+1)$, $u(k)$, and $y(k)$ are the state variable vector, the input vector, and the output vector, respectively. Furthermore, A is the system matrix, B is the control matrix, C is the output matrix, and D is the feed-through matrix. The prediction model can be obtained by combining N equations associated with the instants between $(k+1)$ and $(k+N)$ as expressed below:

$$x(k+1:k+N) = \hat{A}x(k) + \hat{B}u(k:k+N-1) \tag{3}$$

$$x(:) = \hat{A}x(k) + \hat{B}u(:) \tag{4}$$

TABLE I
THREE SWITCHING STATES PER LEG OF THE CONVERTER

S_i	S_{1i}	S_{2i}	$\overline{S}_{1i}$	$\overline{S}_{2i}$
1	ON	ON	OFF	OFF
0	OFF	ON	ON	OFF
-1	OFF	OFF	ON	ON

where

$$\hat{A} = \begin{bmatrix} A \\ A^2 \\ \cdots \\ A^N \end{bmatrix}, \hat{B} = \begin{bmatrix} B & 0 & 0 & 0 \\ AB & B & 0 & 0 \\ \cdots & \cdots & \cdots & \cdots \\ A^{N-1}B & A^{N-2}B & \cdots & B \end{bmatrix} \tag{5}$$

The future error between predicted output and the reference value is minimized by using a predefined cost function, g defined as follows:

$$g = \|x(:)\|^2 + \gamma \|u(:)\|^2 = \left\| \hat{A}x(k) + \hat{B}u(:) \right\|^2 + \gamma \|u(:)\|^2 \tag{6}$$

where γ is the weighting factor.

Taking the derivative of the cost function with respect to u(:) and setting it to zero, the solution is obtained as

$$u(:) = -\left[(\hat{B}^T \hat{B} + \gamma I)^{-1} \hat{B}^T \hat{A} \right] x(k) \tag{7}$$

where only the first vector from the array of the optimally predicted future control inputs in (7) is utilized.

B. Implementation of the FCS-MPC with the PV VSC

The MPC technique requires the accurate modeling of the VSC and the output filter to achieve the desired performance. The voltage expression for each leg of the three-level NPC VSC with respect to the neutral point (N) is given by

$$v_{iN} = S_i \frac{v_{dc}}{2} \tag{8}$$

where the switching function S_i $(i = a, b, c)$ can take the values $1, 0$ or -1 according to the states of the switches of each leg as illustrated in Table I. The common mode voltage, v_{nN} can be subtracted from (8) in order to obtain the phase voltage expression, $\bar{v}_{in}$ given by:

$$\bar{v}_{in} = \bar{v}_{iN} - v_{nN}. \tag{9}$$

The three-phase voltages, v_{abc} and currents, i_{abc} in the stationary abc-frame can be transformed into the corresponding stationary $\alpha\beta$-frame by applying an amplitude invariant Clarke transformation matrix by:

$$v_{\alpha\beta} = \frac{2}{3}(v_{an} + e^{j2\pi/3} v_{bn} + e^{j4\pi/3} v_{cn}). \tag{10}$$

The voltage vectors, $v_{\alpha\beta}$ in the complex domain are presented for a 27-switch configuration pattern in Fig.3

As shown in Fig.1, the ac-terminal of the 3L NPC VSC is connected to the grid through a LCL-filter to suppress the harmonics introduced due to converter switching. The dynamics of the current flowing through the filter inductor in the $\alpha\beta$-frame can be expressed as

$$L_f \frac{d\bar{i}_{f,\alpha\beta}}{dt} = \bar{v}_{i,\alpha\beta} - \bar{v}_{f,\alpha\beta} - R_L \bar{i}_{f,\alpha\beta}. \tag{11}$$

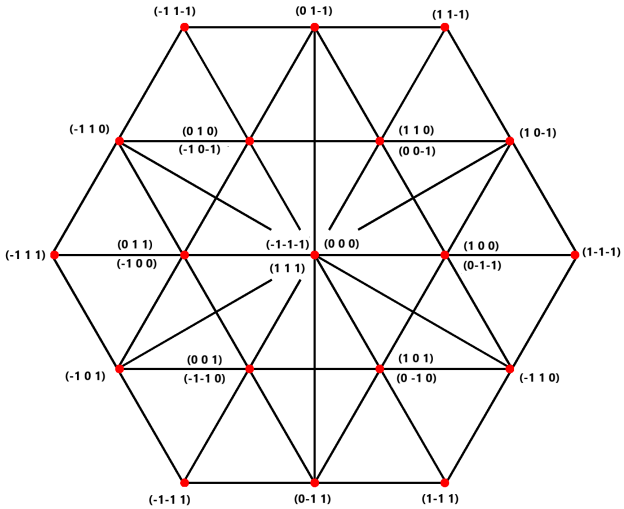

Fig. 3. Space vector diagram showing the possible inverter's switching states

In the context of practical implementation in digital control, the system modeling can be discretized using Forward Euler approximation [25] as

$$\frac{d\bar{i}_{\alpha\beta}}{dt} \approx \frac{i_{\alpha\beta}(k+1) - i_{\alpha\beta}(k)}{T_s}. \tag{12}$$

where T_s is the sampling period. The line current dynamics that estimate the current at the next sample $(k+1)$, can be expressed in discrete form as

$$\bar{i}(k+1) = (1 - \frac{R_L T_s}{L})\bar{i}(k) + \frac{T_s}{L}[\bar{v}_i(k) - \bar{v}_f(k)]. \tag{13}$$

The initial cost function considered for the FCS-MPC control is given by

$$g = (i^*_{f\alpha} - i_{f\alpha})^2 + (i^*_{f\beta} - i_{f\beta})^2 + \gamma_u sw^2 + h_{lim} \tag{14}$$

where the factor sw^2 is used to penalize the switching effort which is again controlled by the weight factor γ_u; h_{lim} is the additional current constraint factor whose value is infinite if the current is higher than the physical inrush current limit of the inverter, i_{lim} else it is considered as zero. The reference current is obtained for each solution as

$$i^*_{\alpha\beta} = \frac{2}{3} T_{dq/\alpha\beta} \cdot P_{set} \cdot \eta \cdot \frac{1}{V_d} \tag{15}$$

where V_d is the real component of the output voltage on the rotating reference frame, η the efficiency of the inverter which can be set to 0.95, P_{set} is the instantaneous power from the PV panels as $P_{set} = v_{dc} i_{pv}$and $T_{dq/\alpha\beta}$ is the Park matrix transformation as given by

$$T_{dq/\alpha\beta} = \begin{bmatrix} \cos(\theta) & -\sin(\theta) \\ \sin(\theta) & \cos(\theta) \end{bmatrix} \tag{16}$$

where θ is the position of the voltage vector $v_{\alpha\beta}$ estimated with a Phase-locked-loop (PLL).

For the dc voltage balance, a new constrain needs to be added in the cost function evaluation. The voltage prediction of each capacitance on the dc side at the next sample time can be given by

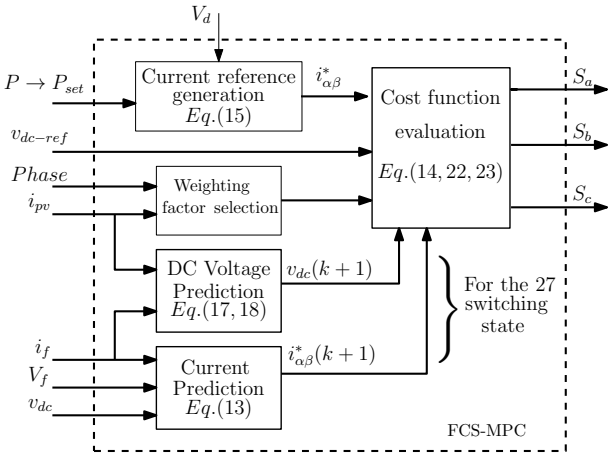

Fig. 4. The proposed FCS-MPC control system.

$$v_{c1}(k+1) = v_{c1}(k) + \frac{(i_{pv}(k) - i_p(k))\,T_s}{C_{dc}} + \frac{i_0(k)T_s}{2C_{dc}} \quad (17)$$

$$v_{c2}(k+1) = v_{c2}(k) + \frac{(i_{pv}(k) + i_n(k))\,T_s}{C_{dc}} - \frac{i_0(k)T_s}{2C_{dc}} \quad (18)$$

where

$$i_0(k) = \overline{S}_0 \bar{i}_{abc} \text{ with } S_{x0}=\begin{cases}1 & if\ S_x = 0\\ 0 & \text{otherwise}\end{cases}; x=\{a,b,c\} \quad (19)$$

$$i_p(k) = \overline{S}_p \bar{i}_{abc} \text{ with } S_{xp}=\begin{cases}1 & if\ S_x = 1\\ 0 & \text{otherwise}\end{cases}; x=\{a,b,c\} \quad (20)$$

$$i_n(k) = \overline{S}_n \bar{i}_{abc} \text{ with } S_{xn}=\begin{cases}1 & if\ S_x = -1\\ 0 & \text{otherwise}\end{cases}; x=\{a,b,c\}. \quad (21)$$

A new constraint is added in the MPC in order to take into account the voltage balance between the capacitance on the dc side as presented in (22) with its weighting factor γ_b.

$$g_{bal} = \gamma_b(v_{c1}(k+1) - v_{c2}(k+1))^2 \quad (22)$$

The PV voltage tracking constrain can be described by

$$g_{pv} = \gamma_v(v_{dc-ref} - (v_{c1}(k+1) + v_{c2}(k+1))^2 \quad (23)$$

where γ_v is the weighting factor.

The schematic of the control systems for the grid-connected single-stage PV system is presented in Fig. 4 where a single step prediction horizon is implemented. The MPPT algorithm presented in next section generates the dc voltage reference, v_{dc-ref}.

III. MPPT Algorithm

As the traditional MPPT algorithms are not able to operate in the single-stage PV integration, an MPPT algorithm has been developed to achieve the desired operation. The algorithm has been embedded with the MPC controller which tracks the maximum power point (MPP). The algorithm can be described in the following three steps.

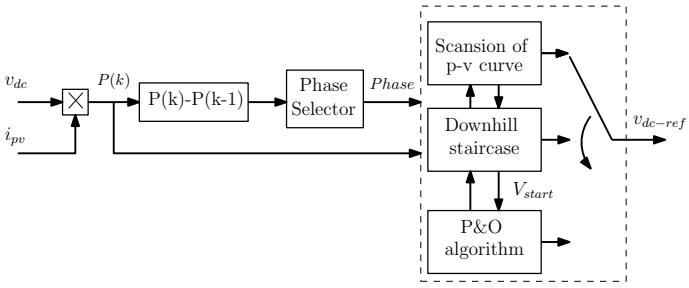

Fig. 5. The improved MPPT block diagram for the single-stage PV system with proposed FCS-MPC.

1) Scanning of the $p-v$ curve forces the dc voltage, v_{dc} to follow the reference dc voltage, v_{dc-ref} as given by

$$v_{dc-ref} = V_{PV}^{Low} + \text{count} * V_{step} \quad (24)$$

in which

$$\text{count} = 1 : (V_{PV}^{High} - V_{PV}^{Low})/V_{step}$$

where V_{PV}^{Low} is the lowest dc voltage allowed for the inverter to have a stable operation, V_{step} is the step voltage during the uphill staircase and V_{PV}^{High} is the upper voltage limit beyond which there is no local MPP. At the end of each voltage step, the value of power will be saved in a vector. The reference voltage of the maximum power point inside the vector is extrapolated. This voltage will refer to the starting point, V_{ref} for the classic P&O algorithm.

2) This phase manages v_{dc-ref} 's jump. v_{dc} will get close to v_{dc-ref} with a downhill voltage step size V_{step}. The voltage step-size can be defined according to the system requirement. The large voltage step takes faster tracking performance with poor dynamic response and vice-versa.
3) In the third-phase when $v_{dc} = v_{dc-ref}$ *i.e.* when the global MPP is almost reached, the MPPT algorithm is switched to the classical P&O algorithm to follow the MPP.

The MPPT algorithm is depicted in Fig. 5. The second phase is the downhill staircase that will be used in two cases, (i) from phase 1 to phase 3, if v_{dc-ref} is far from v_{dc} of the inverter and (ii) during the transition of phase 3 to phase 1, if suddenly a step variation in irradiance occurs, then phase 1 needs to be recalled for a better tracking operation as v_{dc} could be far away from the $p-v$ starting voltage (V_{PV}^{Low}). In the third phase, the P&O algorithm is executed as presented in [21], but ΔV is reduced at the moment that v_{dc} is close to the MPP and the scan of the MPP will be freezed when the power is within $\pm \Delta P$ from the MPP.

This algorithm is described in the following mathematical

TABLE II
CONTROLLER PARAMETERS

Parameters and Description	Value
Sampling time (T_s)	$1 * 10^{-4}$ s
Sampling time of MPPT (T_{MPPT})	$1 * 10^{-3}$ s
Voltage limits in MPPT (V_{PV}^{Low}, V_{PV}^{High})	360, 650 V
Uphill step voltage (V_{step})	20 V
Perturbation in voltage (ΔV)	8 V
Boundary values (ξ_{lower}, ξ_{higher})	2×10^3, 2×10^4
Weighting factors (γ_b, γ_u, γ_v)	8, 8, (8/20/30)

TABLE III
SYSTEM PARAMETERS

Parameter	Description	Value
P_{PV}	maximum power	100 kW
T_{sd}	Simulink discretization time	$1 * 10^{-6}$ s
f_{sw}	Switching frequency	5 kHz
V_{grid}	Utility Grid	25 kV
L_f	Filter inductance	0.7 mH
C_f	Capacitor bank	10 kvar
R_L	Resistive filter components	0.00377 Ω
C_{dc}	Capacitance on DC side	3 mF

expressions:

$$\text{MPP left side}: \frac{\partial P_{PV}}{\partial v_{PV}} > 0 \Rightarrow V_{ref} = V_{ref} + \Delta V \quad (25)$$

$$\text{MPP right side}: \frac{\partial P_{PV}}{\partial v_{PV}} < 0 \Rightarrow V_{ref} = V_{ref} - \Delta V \quad (26)$$

$$\text{At the MPP}: \frac{\partial P_{PV}}{\partial v_{PV}} = 0 \Rightarrow V_{ref} = V_{ref} \quad (27)$$

The amount of power, which identifies a step irradiance change is set with two different boundaries ξ during phase 3 in order to ensure a more robust tracking performance. In this context, the highest boundary level of ξ is set during the MPP search, to avoid the re-calling of phase 1. When the MPP is found, the algorithm becomes more sensible about step irradiance changes and therefore, the smaller boundary level of ξ is imposed.

The time of each phase depends on the size of the dc capacitance and the capability of the control to follow the reference voltage. As presented in [26], the dc-link capacitor can be designed as

$$C_{dc} = \frac{S}{2 w_g V_{dc} \overline{V}_{dc}} \quad (28)$$

where S is the rated power of the inverter, V_{dc} is the average voltage, $\overline{V}_{dc}$ is the maximum permissible voltage ripple and w_g is the utility frequency which is equal to $2\pi f_g$.

Without any modification of the proposed control system, under low/null irradiance, the following problems occur: (i) forcing the system to work at V_{PV}^{Low}, which leads to current distortion as the control system asks for a large current from the grid to control the v_{dc} as the current from the PV is almost 0; (ii) during the first $p - v$ scan, the system is not able to follow v_{dc-ref} as the input power is not enough to ensure a fast charging of the input capacitance. In order to solve these two issues the following modifications have been implemented

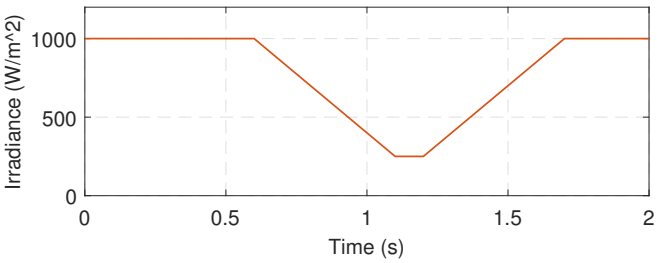

Fig. 6. Solar irradiance applied to test performance of the PV system.

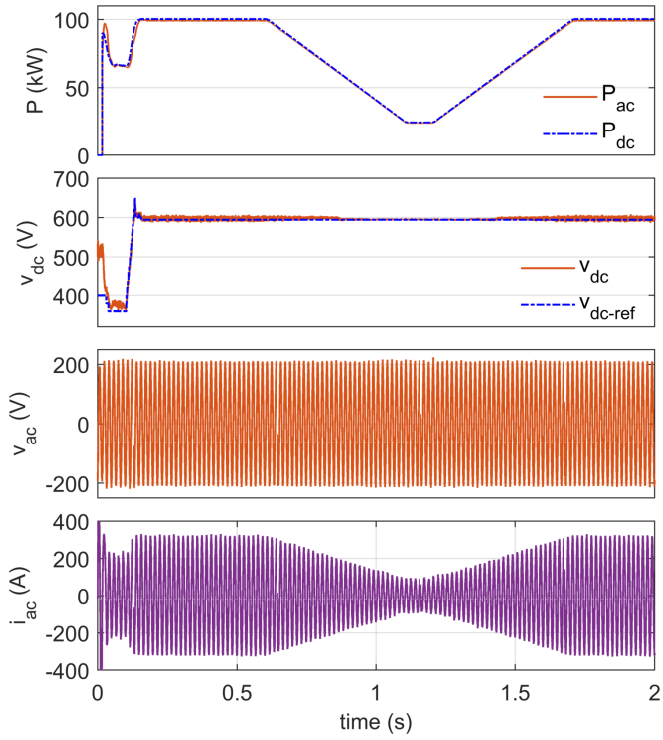

Fig. 7. Simulation results of single-stage PV connection with the proposed control as shown in Fig. 2: (i) output power, (ii) the dc-bus voltage, (iii) the PCC voltage and (iv) ac output current of the inverter in response to the irradiance applied as shown in Fig. 6.

in the MPPT algorithm: (i) when the input power is less than 10% of the rated power, the MPPT algorithm runs a new phase where v_{dc-ref} follows the v_{dc} thus, the input voltage is free to evolve and approaches to the stable working point where v_{dc} is higher than the V_{PV}^{high} and the current is null; (ii) phase 1 of the MPPT algorithms is disabled as long as the power from the PV is less then 10% of the rated power.

IV. SIMULATION RESULTS

A. Investigated system configuration

In order to verify the performance, the proposed single-stage grid-connected PV system has been implemented in MATLAB/Simulink and the SimPower Toolbox. The detailed model of a three-level 100-kW grid-connected PV array developed by MathWorks and HydroQuebec [27] has been taken

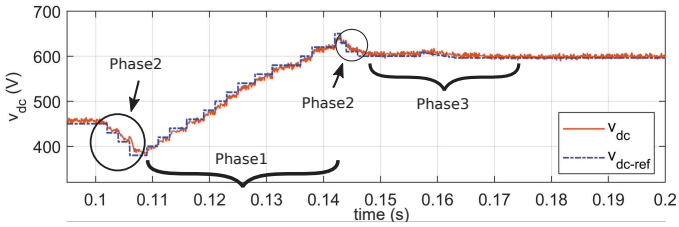

Fig. 8. Zoomed view of the tracking phases of proposed algorithm

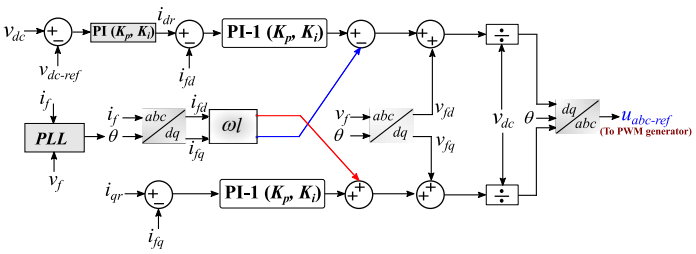

Fig. 9. Schematic of the standard PI-current controller.

as the benchmark model. The benchmark model of the grid-connected PV system consists of PV panels, a dc-dc boost converter and a three-level NPC inverter. The widely-used vector control is used to control the inverter which has an inner-loop current control and outer-loop dc voltage control. The MPPT algorithm controls the switch of the dc-dc boost converter to obtain the desired level of dc voltage at the PV side to extract maximum power. The SunPower SPR-305E model is used to emulate the PV panel. The PV plant has 5 series-connected modules and 66 parallel strings with a nominal rated power of 100 kW.

The proposed control with the updated MPPT technique has been implemented in the inverter of the benchmark model. The dc-dc boost converter is removed from the benchmark model to make it a single-stage conversion system. Since the dc-dc boost converter is removed, the PV string setting is changed to an 11 series panel with 30 parallel strings to achieve the same rated power as of the bench mark model. The parameters of the investigated single-stage PV system and the proposed controller are given in Table II and III, the utility grid is connected to a 100 kVA - (260 V/25 kV) three-phase coupling transformer and it is characterized by a 25 kV distribution feeder plus a 120 kV equivalent transmission system.

B. Simulation comparison with the standard control system

The purpose of this simulation is to evaluate the capability of the proposed system to work within all ranges of irradiance, keeping stable output signals as the conventional PI current control with the dc-dc boost converter presented in Fig. 1. This feature is not obvious without the classic boost converter as the C_{dc} and filter parameter are set based on an average value of power, and the input voltage on the inverter is also not fixed. Therefore, the amplitude of the voltage vector applied from the inverter will be variable. The MPPT algorithm applied in the classical solution is the well-know Incremental Conductance algorithm [21], which will not be able to work under partially shaded conditions but is more stable with uniform irradiance

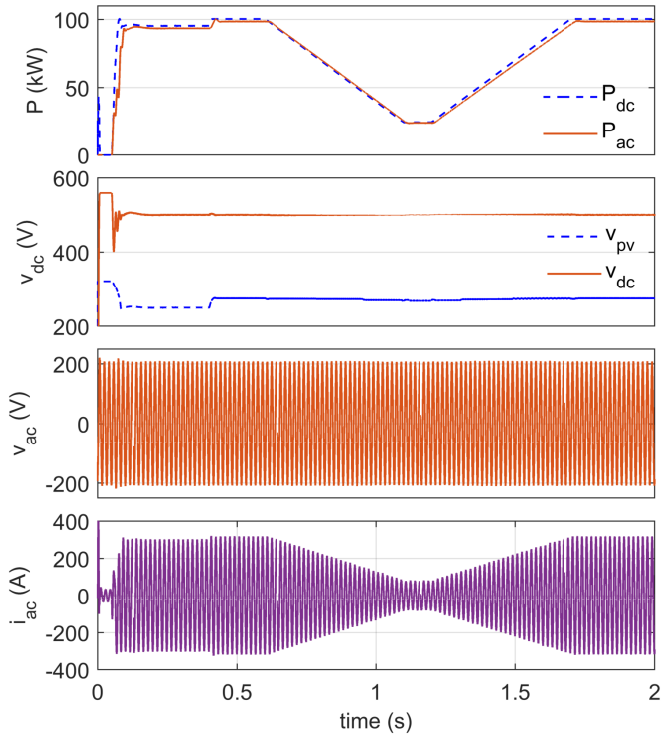

Fig. 10. Simulation results of two-stage PV connection with the classical vector control as shown in Fig. 1: (i) output power, (ii) the dc-bus voltage, (iii) the PCC voltage and (iv) ac output current of the inverter in response to the irradiance applied as shown in Fig. 6.

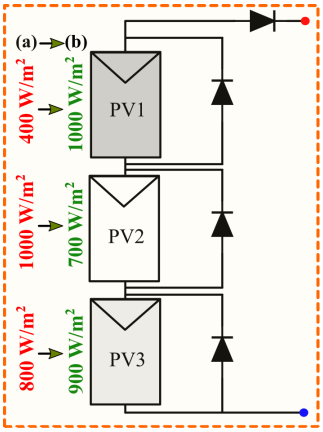

Fig. 11. PV configuration to test the partially shaded condition. The irradiance has been changed from $[400\ 1000\ 800]\ w/m^2$ to $[1000\ 700\ 900]\ w/m^2$.

input. The MPPT parameters for the simulation comparison with the PI-based control system are presented as follows: V_{PV}^{Low} and V_{PV}^{High} are set to 360 and 650 V, respectively; V_{step} and ΔV are 20 V and 8 V; ξ_{lower} and ξ_{higher} are 2×10^4 and 2×10^3, respectively and ΔP is set to 50 W.

A simulation has been carried out for the irradiance profile shown in Fig. 6, and the obtained output power, dc-link voltage, voltage at the PCC and ac output current are shown in Fig. 7. The simulation starts at $t = 0$ s, the MPPT is enabled and searches for the maximum power point. As can be

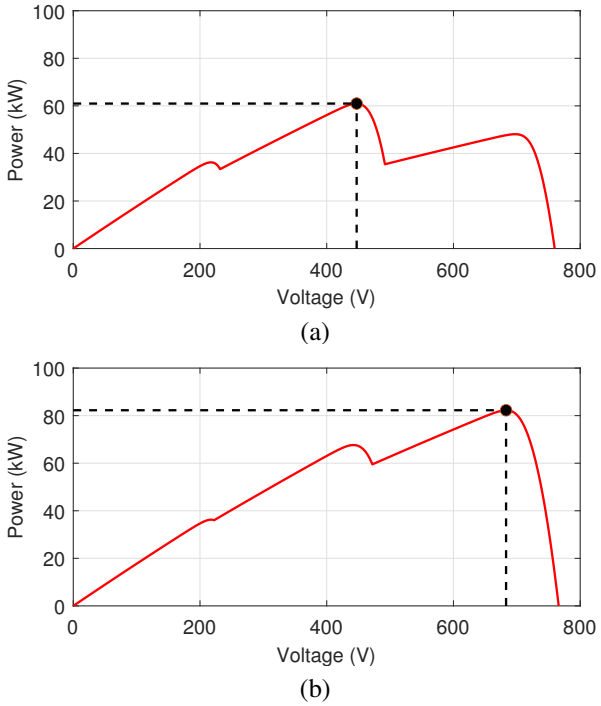

Fig. 12. Ideal $p-v$ curve with irradiance set equal to $[400 \cdot 1000 \cdot 800]$ and $[1000 \cdot 700 \cdot 900]$.

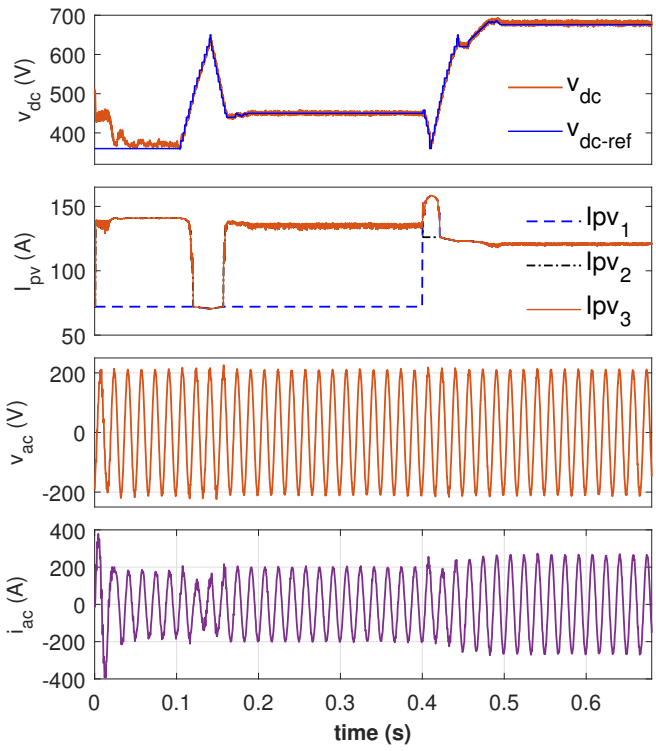

Fig. 13. Simulation results with the proposed control: a) dc voltage, b) PV currents, c) output ac voltage and d) output current.

seen, within some ms, the algorithm can track the MPP and send the power according to the solar irradiance. The FCS-MPC stabilizes the dc-link voltage and follows the reference to extract the maximum power. It is worth highlighting that a more accurate dc voltage tracking with the proposed control, Fig. 7, is obtained with the value of γ_u and γ_b equal to each other for the high irradiance and with an increased value of γ_v during low irradiance. For more clarity, the zoomed view of the dc-link voltage is presented in Fig. 8, where the tracking of the dc-link voltage to the reference value during all three phases are clearly visible. The ac voltage is very stable and does not have any impact on the variation of the output power. The output current follows the output power. Overall the performance of the single-stage PV system is very good. The average time to find the MPP is equal to $55\,ms$ for each solution. With the additional constraints about the dc voltage balance reported in (22) in the proposed controller, the dc voltage capacitance is maintained as stable as in the benchmark model, with an overlapped peak to peak signal equal to $10\,V$. It is worth mentioning that three constant values of the weighting factor γ_v are chosen in this work based on the amount of injected power which is directly proportional to the i_{pv}. These values are obtained by the trial-and-error method with the FCS-MPC algorithm to achieve the best tracking operation of the single-stage PV system. γ_v is kept fixed at 8 when the injected dc power P_{dc} is more than 50% of the rated power, attains the value 20 when P_{dc} is in the range of 35-50%, and shifts to the value 30 when P_{dc} falls between 0-35% of the rated power. On the other hand, the value of the weighting factor γ_b is instead kept constant at 8 (after the MPPT algorithm is enabled) to give more importance to the

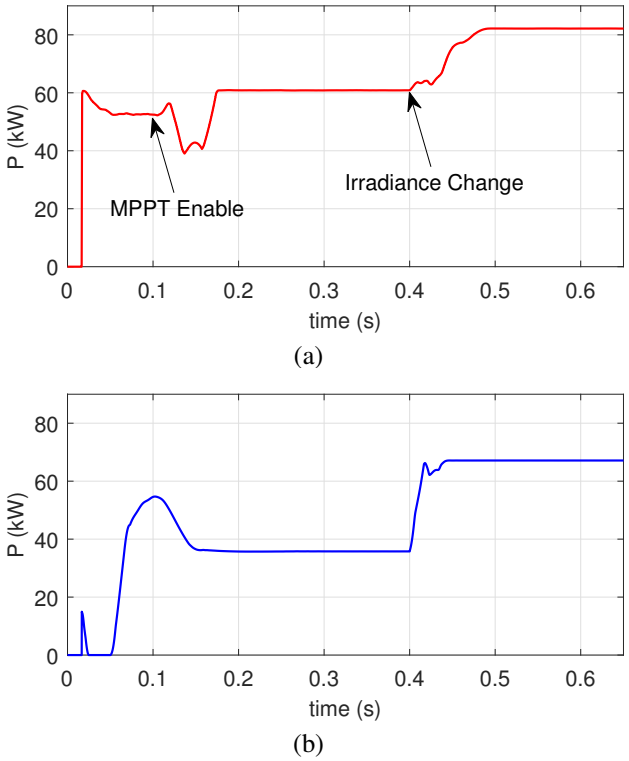

Fig. 14. Output power in response to a step irradiance change from $[400 \quad 1000 \quad 800]\ w/m^2$ to $[1000 \quad 700 \quad 900]\ w/m^2$ at $0.4s$: a) the proposed system and b) the benchmark model.

TABLE IV
EFFICIENCY EVALUATION OF THE PV SYSTEM

% Output power	5%	10%	20%	30%	50%	100%	$\eta_{EU}(\%)$
-	5kW	10kW	20kW	30kW	50kW	100kW	-
w_f	0.03	0.06	0.13	0.1	0.48	0.2	-
Benchmark model	91.23	94.02	96.01	95.98	96.2	96.7	95.97
Proposed system	94.31	96.01	97.89	98.63	98.5	98.97	98.25

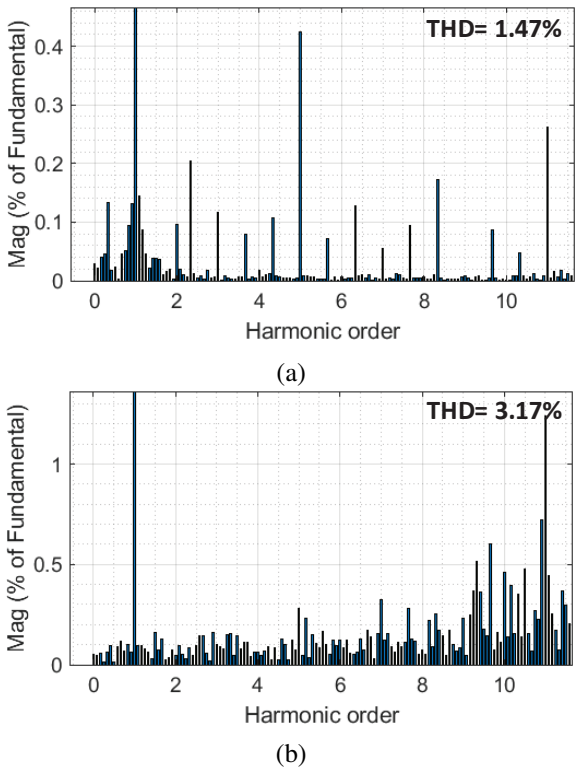

Fig. 15. Harmonic spectra of output current a) Benchmark model, b) Single-stage model using proposed controller.

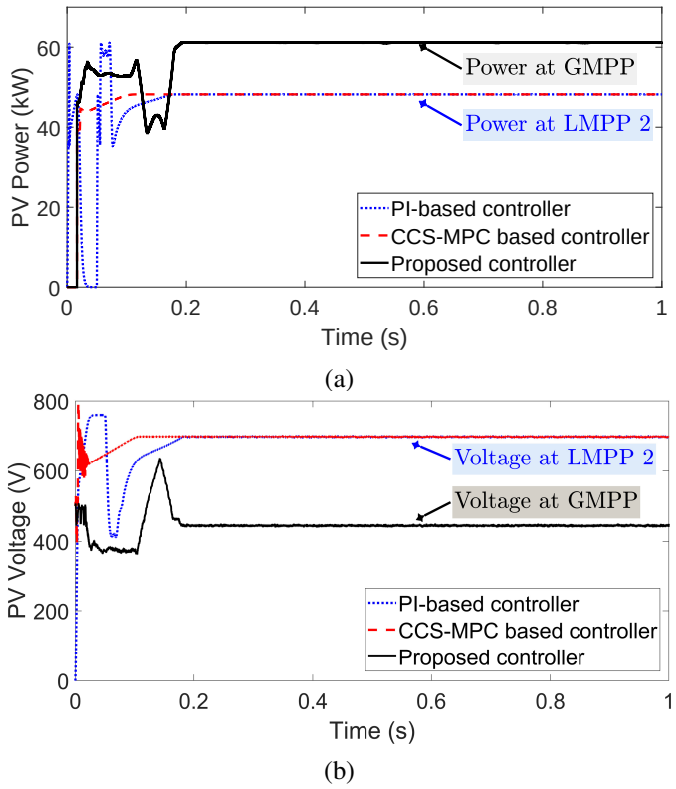

Fig. 16. Comparative simulation results of single-stage PV connection with the classical vector control and CCS-MPC combined with P&O MPPT algorithm, (a) PV power, (b) PV voltage.

dc voltage tracking.

In order to compare the performance of the proposed control with the benchmark model with the standard vector PI control, a simulation is carried out and the obtained results are presented in Fig. 10. The schematic of the implemented standard current controller for the benchmark model is depicted in Fig. 9, where phase-locked-loop (PLL), dc voltage regulator, and current regulator are the three main control loops for the 3-level NPC. By comparing the result of Fig. 7 and Fig. 10, the active power from the benchmark model and the proposed systems are the same throughout the PV system's working range. There is no noticeable difference in time-domain response in terms of the performance of the two systems. The only noticeable difference is the total harmonic distortion (THD) level in the current waveform. The THD at the rated power is 1.47% for the benchmark model while it is 3.17% for the proposed control system as presented in Fig. 15. A higher THD for the proposed system is expected as the inverter LCL-filter for the benchmark model is designed and optimized for the standard vector control, while the same filter is adopted for the proposed control system.

C. Comparative performance in partially shaded condition

To investigate partially shaded conditions by providing different solar irradiance, the PV panel has been connected as shown in Fig. 11. In order to maintain the same rated dc voltage and output power as described in IV-A, each panel is composed of 4 series-connected modules and 30 parallel strings. A diode has been connected in parallel with PV panels to maintain the maximum current flow from PV panels. The single-stage PV system and the benchmark system are tested under the sudden irradiance changing condition from $[400 \quad 1000 \quad 800]\ w/m^2$ to $[1000 \quad 700 \quad 900]\ w/m^2$ at $0.4s$. The Ideal $p-v$ curves with these irradiance sets are shown in Fig. 12. It can be seen from Fig. 12 that the maximum powers are 60.9 kW and 82.2 kW with corresponding PV voltage of 447.2 V and 683 V, respectively. A simulation has been carried out for this irradiance change. The events of the simulation are in the following steps: the PV panels are connected since the beginning and at $t = 0.1\ s$, the MPPT algorithm is enabled and starts to scan the $p-v$ curve. The simulation results for the single-stage PV system are presented

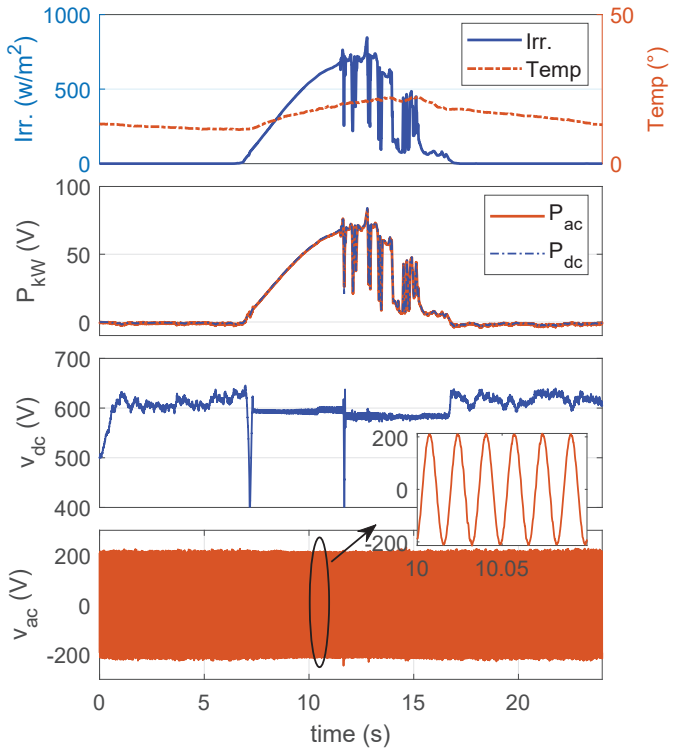

Fig. 17. Simulation results of the proposed single-stage FCS-MPC control for solar inverter with a radiation and temperature on typical day.

in Fig. 13. The proposed MPPT algorithm can track the MPP within 0.08 s. The distortion in current i_{ac} in Fig. 13 is related to the moment when one of the PV approaches to the shaded conditions and the currents from the PVs are not equal to each other. This effect is presented in the PV current, i_{pv} in Fig. 13 in which it can be distinguished the partially shaded condition when more than one current shape is present in the system. From the simulation, it can be seen that the output signals at the MPP working point are difficult to stabilize when the currents from the PVs are different from each other, as the input current from the power source is less stable. The output power is presented in Fig.14(a). At the steady-state, the extracted power is the same as shown in Fig.12 i.e equal to 60.8 and 82.16 kW, respectively. The proposed FCS-MPC with the improved MPPT algorithm works for the partially shaded condition. A similar simulation for the benchmark model has also been carried out, and the obtained output power is shown in Fig. 14(b). The steady-state output power for the benchmark model is 35.79 kW and 67.13 kW, while the global MPP is at 60.9 kW and 82.2 kW respectively. The benchmark model failed to find the global MPP under partially shaded conditions.

Furthermore, the performance of the proposed control is also compared with two other controllers in terms of effective MPPT tracking, i.e., (i) a PI current controller combined with the perturb and observe (P&O) MPPT technique and (ii) the continuous control set model predictive control (CCS-MPC) combined with the P&O MPPT technique, considering the works of literature [22]–[24]. The partial shading test case

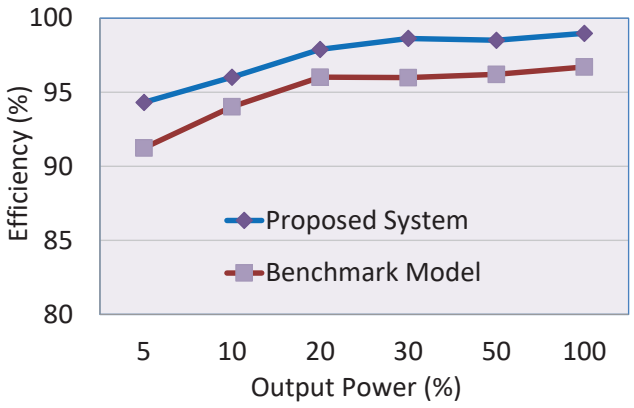

Fig. 18. European efficiency computation of the grid-connected PV system.

is carried-out by considering the PV system configuration shown in Fig. 11 for the irradiation pattern presented in Fig. 12(a). The resulted power and voltage waveforms under the considered irradiation pattern are depicted in Fig. 16. As can be seen in Fig. 12(a) and Fig. 16, the GMPP is successfully tracked by the proposed FSC-MPC and improved MPPT technique, while the PI-based controller and CCS-MPC controller combined with the P&O algorithm are settled at the LMPP2 (47 kW, 700 V). This proves the effectiveness of the proposed controller in extracting the maximum power and maintaining the stable dc-link voltage irrespective of the irradiation pattern.

D. Simulation with realistic irradiance data

In this subsection, the control has been tested for a real irradiance and temperature data set for a typical winter day in Australia as shown in the top plot of Fig.17 [28]. The simulation has been tested for the system described in sub-section IV-A. The simulation result is presented in Fig.17. The proposed technique can ensure a high power efficiency extrapolation, within the entire range of irradiance and even with step irradiance change. The v_{dc} is able to follow the MPP dynamically, showing the effectiveness of the dc voltage control directly in the FCS-MPC current control.

E. Efficiency evaluation

The Weighted European efficiency (η_{EU}) is considered as one of the standard efficiency computation factors for any grid-connected PV systems. In this method, the efficiency at different operating points is considered, then those points are multiplied with the corresponding pre-defined weight factors (w_f) [29]. The overall efficiency of both the single-stage and double-stage PV system are summarized in Table IV by considering the same linear irradiation changing pattern. It is evident from Fig. 18 that the overall efficiency of the single-stage PV system controlled by the proposed FCS-MPC algorithm is comparatively high in the entire operating range.

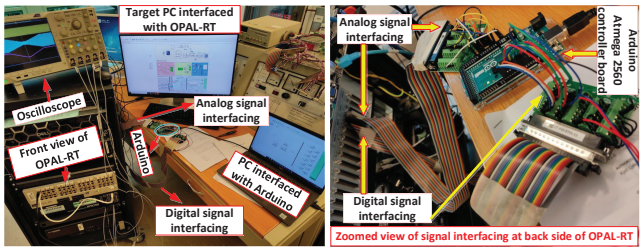

Fig. 19. C-HIL setup developed in the laboratory

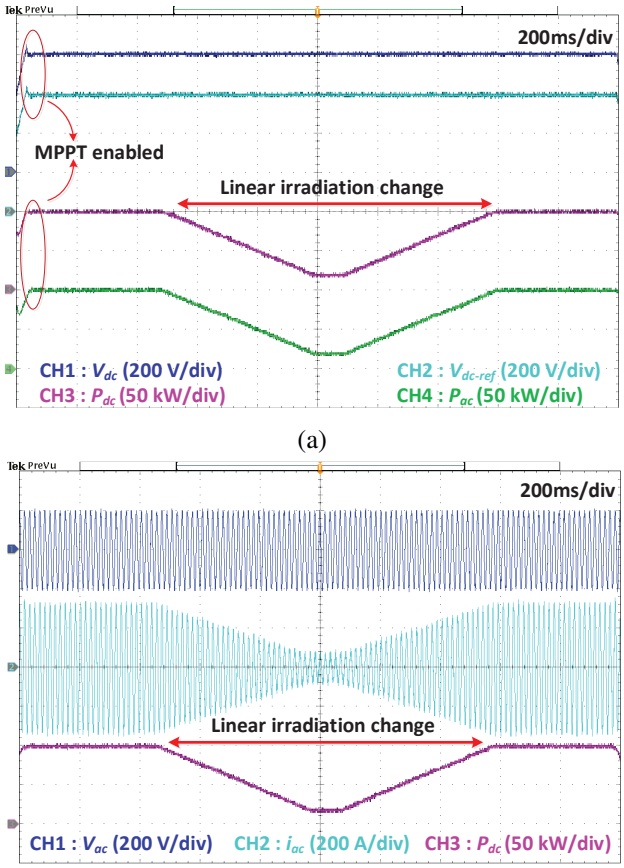

Fig. 20. C-HIL results using FCS-MPC control a) dc voltage and output power, b) output ac voltage, current and dc power

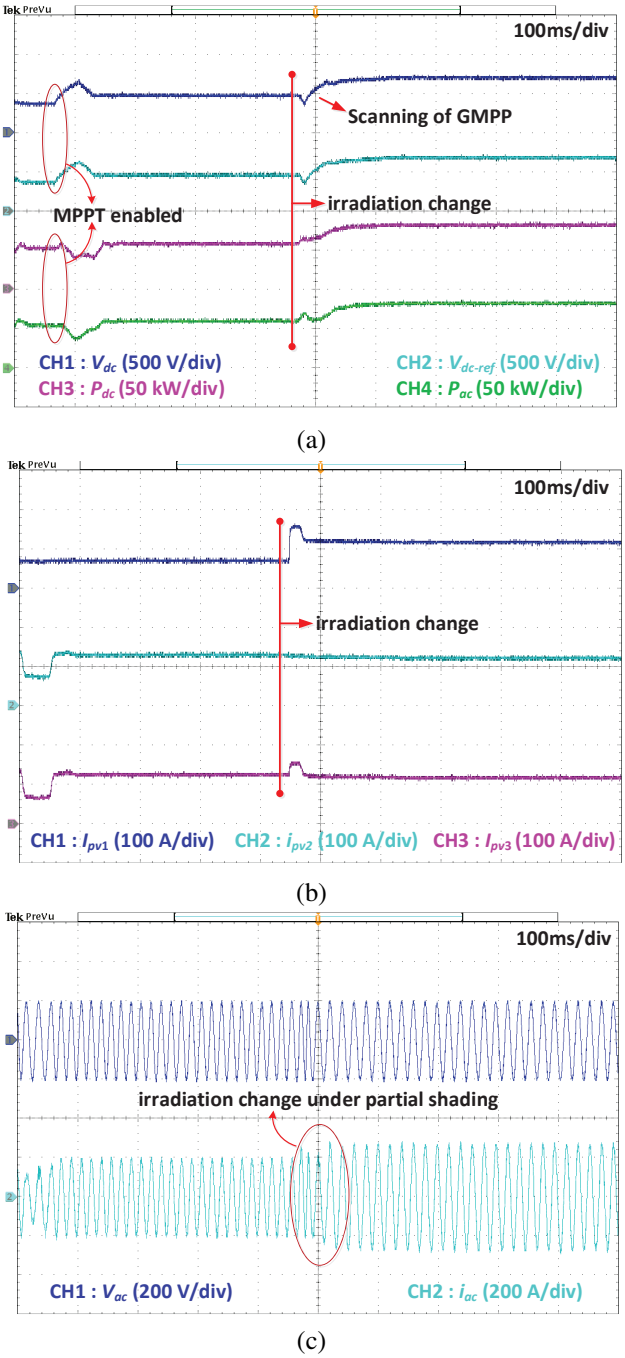

Fig. 21. C-HIL results under partial shading a) dc voltage and output power, b) PV array currents, c) output ac voltage and current

V. Experimental Results

To further verify the performance of the proposed control system for the single-stage grid-connected PV system, experimental tests according to a control hardware-in-loop (C-HIL) approach have been performed. The C-HIL setup developed in the laboratory works with the combined interaction of an OPAL-RT platform and Arduino Mega 2560 controller board. The complete system runs in a hardware synchronization mode with the physical clock time, and also offers the electrical system and its controller to run with a wide range of sampling times. The laboratory setup picture is shown in Fig. 19. The electrical physical system undertaken for this work is modeled inside the OPAL-RT platform considering the standard library tools. The necessary analog feedback signals are sent from this OPAL-RT platform to the Arduino controller board via analog interfacing board. The Arduino board generates the desired PWM signals by estimating the proposed control algorithm. Moreover, the Arduino controller board is directly interfaced with the MATLAB/Simulink environment and the control part is directly built into the board through a Simulink model. In line with this, all the desired signals of the proposed system are collected at the analog-out pins of the OPAL-RT and are captured with an external oscilloscope. In this way, the control loop is closed as in the real full-scale system, and representative results can be obtained.

In line with the simulation analysis, the proposed controller for the single-stage PV system is tested under similar linear irradiation changing condition and partial shading conditions. Fig. 20 depicts the output findings when the irradiance drops linearly from 1000 W/m^2 to 200 W/m^2. After the MPPT algorithm is enabled in the first phase of experimentation, it starts searching for the MPP and tracks the MPP within a short fraction of time thereby feeding the proportional power to the grid as shown in Fig. 20(a). Moreover, the FCS-MPC stabilizes the dc-link voltage and follows the reference to extract the optimum power. Fig. 20(b) indicates that the ac voltage waveform is very stable irrespective of the variation in power level although the output current follows the output power waveform magnitude with negligible distortions.

Further, the results are also obtained under a partial shading scenario when the irradiance level changes from [400 1000 800] W/m^2 to [1000 700 900] W/m^2 and presented in Fig. 21. When the MPPT is enabled, it scans the $p-v$ curve and quickly settles at the MPP indicating the fast operation of the proposed algorithm. Moreover, the global MPP (GMPP) is also tracked within a short interval of time as the dc voltage, and the power curve are settled at their new desired steady values, which are evident from Fig. 21. Further, small distortions in the output currents are observed, which are in fact related to the moment when one of the PV approaches to the shaded condition and the currents from the PVs are not equal. However, all the three PV currents get settled at the same value when the GMPP is tracked. This effect can be visualized from Fig. 21(b) and Fig. 21(c). Throughout this test case, the output voltage waveform remains unaffected.

VI. Conclusion

This paper presents an efficient FCS-MPC control technique for the single-stage grid-tied PV system. The addition of a new constraint to the cost factor equation makes the FCS-MPC more adaptive in tracking the dc-link reference voltage value. The adaptive weight factor is the key parameter that stabilizes the output signals once the MPPT is reached. A comparative simulation analysis demonstrates the effectiveness of the proposed control technique in tracking the global maximum power point under partially shaded and step irradiance change conditions. The results for partially shaded, step and linear irradiance changes prove the feature of the system to work in the entire $p - v$ characteristic, ensuring a stable output signal and the maximum power extraction during the transient condition.

References

[1] R. Lacal Arantegui and A. Jager-Waldau, "Photovoltaics and wind status in the european union after the paris agreement," Renew. Sust. Energ. Rev., vol. 81, pp. 2460 – 2471, 2018.

[2] Y. Zhu, J. Yao, and D. Wu, "Comparative study of two stages and single stage topologies for grid-tie photovoltaic generation by pscad/emtdc," in 2011 International Conference on Advanced Power System Automation and Protection, vol. 2, 2011, pp. 1304–1309.

[3] Ankit, S. K. Sahoo, S. Sukchai, and F. F. Yanine, "Review and comparative study of single-stage inverters for a pv system," Renew. Sust. Energ. Rev., vol. 91, pp. 962–986, 2018.

[4] B. Sahan, A. N. Vergara, N. Henze, A. Engler, and P. Zacharias, "A single-stage pv module integrated converter based on a low-power current-source inverter," IEEE Trans. Ind. Electron., vol. 55, no. 7, pp. 2602–2609, 2008.

[5] P. Shah, I. Hussain, and B. Singh, "Fuzzy logic based fogi-fll algorithm for optimal operation of single-stage three-phase grid interfaced multifunctional secs," IEEE Trans. Ind. Informat., vol. 14, no. 8, pp. 3334–3346, 2018.

[6] J. He and Y. W. Li, "Generalized closed-loop control schemes with embedded virtual impedances for voltage source converters with lc or lcl filters," IEEE Trans. Power Electron., vol. 27, no. 4, pp. 1850–1861, 2012.

[7] J. Rocabert, A. Luna, F. Blaabjerg, and P. RodrÃguez, "Control of power converters in ac microgrids," IEEE Trans. Power Electron., vol. 27, no. 11, pp. 4734–4749, 2012.

[8] F. Blaabjerg, R. Teodorescu, M. Liserre, and A. V. Timbus, "Overview of control and grid synchronization for distributed power generation systems," IEEE Trans. Ind. Electron., vol. 53, no. 5, pp. 1398–1409, 2006.

[9] S. Bayhan and H. Abu-Rub", ""40 - predictive control of power electronic converters"," in "Power Electronics Handbook", "fourth edi- tion" ed., M. H. Rashid", Ed. "Butterworth-Heinemann", "2018", pp. "1325 – 1338".

[10] J. Hu, J. Zhu, G. Lei, G. Platt, and D. G. Dorrell, "Multi-objective model- predictive control for high-power converters," IEEE Trans. Energy Convers., vol. 28, no. 3, pp. 652–663, 2013.

[11] A. A. Ahmed, B. K. Koh, and Y. I. Lee, "A comparison of finite control set and continuous control set model predictive control schemes for speed control of induction motors," IEEE Trans. Ind. Informat., vol. 14, no. 4, pp. 1334–1346, 2018.

[12] P. C, J. R, S. V, and L. G. F, "Predictive control of a three-phase ups inverter using two steps prediction horizon," in 2010 IEEE Int. Conf. Ind. Technol., 2010, pp. 1283–1288.

[13] T. Geyer and D. E. Quevedo, "Performance of multistep finite control set model predictive control for power electronics," IEEE Trans. Power Electron., vol. 30, no. 3, pp. 1633–1644, 2015.

[14] T. Geyer and D. E. Quevedo, "Performance of multistep finite control set model predictive control for power electronics," IEEE Trans. Power Electron., vol. 30, no. 3, pp. 1633–1644, 2015.

[15] J. M. C. Geldenhuys, H. du Toit Mouton, A. Rix, and T. Geyer, "Model predictive current control of a grid connected converter with lcl-filter," in 2016 IEEE 17th Workshop on Control and Modeling for Power Electronics (COMPEL), 2016, pp. 1–6.

[16] M. Hamdi, M. Hamouda, L. Sbita, and K. Al-Haddad, "Fcs-mpc for grid-tied three-phase three-level npc inverter with experimental validation," in 2017 International Conference on Green Energy Conversion Systems (GECS), 2017, pp. 1–6.

[17] J. Gao, C. Gong, W. Li, and J. Liu, "Novel compensation strategy for calculation delay of finite control set model predictive current control in pmsm," IEEE Trans. Ind. Electron., vol. 67, no. 7, pp. 5816–5819, 2020.

[18] C. A. Rojas, J. Rodriguez, F. Villarroel, J. R. Espinoza, C. A. Silva, and M. Trincado, "Predictive torque and flux control without weighting factors," IEEE Trans. Ind. Electron., vol. 60, no. 2, pp. 681–690, 2013.

[19] Z. Zhang, H. Fang, F. Gao, J. RodrÃguez, and R. Kennel, "Multiple-vector model predictive power control for grid-tied wind turbine system with enhanced steady-state control performance," IEEE Trans. Ind. Electron., vol. 64, no. 8, pp. 6287–6298, 2017.

[20] T. Tarczewski and L. M. Grzesiak, "Constrained state feedback speed control of pmsm based on model predictive approach," IEEE Trans. Ind. Electron., vol. 63, no. 6, pp. 3867–3875, 2016.

[21] S. Jain and V. Agarwal, "Comparison of the performance of maximum power point tracking schemes applied to single-stage grid-connected photovoltaic systems," IEE Proc. Electric Power Appli., vol. 1, pp. 753 – 762, 10 2007.

[22] D. Sera, L. Mathe, T. Kerekes, S. V. Spataru, and R. Teodorescu, "On the perturb-and-observe and incremental conductance mppt methods for pv systems," IEEE J. Photovolt., vol. 3, no. 3, pp. 1070–1078, 2013.

[23] C. Xue, L. Ding, and Y. Li, "Ccs-mpc with long predictive horizon for grid-connected current source converter," in 2020 IEEE Energy Conv. Congress and Exposition, 2020, pp. 4988–4993.

[24] H. Chen, D. Wang, S. Tang, X. Yin, J. Wang, and Z. J. Shen, "Continuous control set model predictive control for three-level flying capacitor boost converter with constant switching frequency," IEEE J. Emerg. Sel. Topics Power Electron., vol. 9, no. 5, pp. 5996–6007, 2021.

[25] T. Dragicevic, "Model predictive control of power converters for robust and fast operation of ac microgrids," IEEE Trans. Power Electron., vol. 33, no. 7, pp. 6304–6317, 2018.

[26] E. A. B. Munwar Ayaz Memon, Ghullam Mustafa Bhutto, "Sizing of dc- link capacitor for a grid connected solar photovoltaic inverter," vol. 13, pp. 2272–2281, 2020. 12

[27] P. Giroux, G. Sybille, C. Osorio, and S. Chandrachood, "Detailed model of a 100-kw grid-connected pv array," accessed 01 Feb 2021.

[28] M. Islam, F. Yang, and M. Amin, "Dynamic control of grid-connected microgrids for tie-line smoothing," Int. Trans. Electr. Energy Syst., vol. 30, no. 11, p. e12557, 2020.
[29] M. N. H. Khan, M. Forouzesh, Y. P. Siwakoti, L. Li, T. Kerekes, and F. Blaabjerg, "Transformerless inverter topologies for single-phase photovoltaic systems: A comparative review," IEEE J. Emerg. Sel. Topics Power Electron., vol. 8, no. 1, pp. 805–835, 2020.

Vanti Simone (Student Member, IEEE) received the B.Sc. and M.Sc degree in mechatronic engineering from the University of Padova in 2018 and 2021, respectively.

During January to May 2021, he was with the Department of Electrical Power Engineering, Norwegian University of Science and Technology, Norway, for his master thesis project. Currently, he is working with the Coesia in Italy as a Mechatronic Engineering in the R&D department. His research interest includes on power electronics application to power system, application of artificial intelligence in power electronics system and robust control theory for power electronics system.

Prabhat Ranjan Bana (Student Member, IEEE) received the B.Tech. degree in electrical engineering from Parala Maharaja Engineering College, Berhampur, India, in 2016, and the M.Tech. degree in power and energy systems specialization from the National Institute of Technology (NIT) Meghalaya, Shillong, India, in 2019. He is currently working toward the Ph.D. degree with the Department of Electric Power Engineering, Norwegian University of Science and Technology, Trondheim, Norway.

During January to March 2019, he was a Visiting Scholar with the Cardiff University, Cardiff, U.K., funded through the Joint U.K.-India Clean Energy (JUICE) two months exchange program scheme. From July 2019 to February 2020, he was a Research Associate with NIT Meghalaya. His research interests include multilevel inverters, photovoltaic systems, and artificial intelligence based control of power elctronics system.

Salvatore D'Arco received the M.Sc. and Ph.D. degrees in electrical engineering from the University of Naples "Federico II," Naples, Italy, in 2002 and 2005, respectively.

From 2006 to 2007, he was a postdoctoral researcher at the University of South Carolina, Columbia, SC, USA. In 2008, he joined ASML, Veldhoven, the Netherlands, as a Power Electronics Designer consultant, where he worked until 2010. From 2010 to 2012, he was a postdoctoral researcher in the Department of Electric Power Engineering at the Norwegian University of Science and Technology (NTNU), Trondheim, Norway. In 2012, he joined SINTEF Energy Research where he currently works as a Senior Research Scientist. He is the author of more than 130 scientific papers and is the holder of one patent. His main research activities are related to control and analysis of power-electronic conversion systems for power system applications, including real-time simulation and rapid prototyping of converter control systems.

Mohammad Amin (M'11-SM'20) received the B.Sc. degree in electrical and electronic engineering from Chittagong University of Engineering and Technology, Bangladesh, in 2008, the M.Sc. degree in electric power engineering from Chalmers University of Technology, Sweden, in 2011 and the Ph.D. degree in engineering cybernetics from Norwegian University of Science and Technology, Norway, in 2017.

From 2008 to 2013, he was with the Department of Electrical and Electronic Engineering, International Islamic University Chittagong, Bangladesh. In 2015, he was a Ph.D. Visiting Scholar with the Wind Power Research Center, Shanghai Jiao Tong University, Shanghai, China. From 2017 to 2019, he was a Senior Research Associate with the Department of Electrical and Computer Engineering, Illinois Institute of Technology, Chicago, IL, USA. Currently, Dr. Amin is an Associate Professor with the Department of Electric Power Engineering at Norwegian University of Science and Technology. He is the recepient of the 2018 IEEE JESTPE First Prize Paper Award from IEEE Power Electronics Society and The 2020 Premium Award for best paper in IET Generation, Transmission & Distributio. His research interest include on power electronics application to power system, application of artificial intelligence in power electronics system, robust integration of wind and solar energy, high voltage direct current (HVDC) transmission, microgrid, smart grids, and robust control theory for power electronics system.